Low-temperature transport properties of Ta$_x$N thin films (0.72 ≤ x ≤ 0.83)

Low-temperature transport properties of Ta$_x$N thin films ($0.72 \leqslant x \leqslant 0.83$)

Miroslav Očko[1], **Sanja Žonja**[1,2], **G L Nelson**[3], **J K Freericks**[3], **Lei Yu**[4] **and N Newman**[5]

[1] Institute of Physics, Bijenička 46, HR-10002 Zagreb, Croatia

[2] Faculty of Electrical Engineering and Computing, Unska 3, HR-10000 Zagreb, Croatia

[3] Department of Physics, Georgetown University, 37th and O Sts. NW, Washington, DC 20057, USA

[4] Department of Physics and Astronomy, Rutgers, The State University of New Jersey,
136 Frelinghuysen Road, Piscataway, NJ 08854-8019 USA

[5] School of Materials, Arizona State University, Tempe, AZ, USA

E-mail: ocko@ifs.hr

Abstract

We report on low-temperature (4–320 K) transport properties of Ta$_x$N thin films deposited on an amorphous SiO$_2$ substrate. In this work, Ta$_x$N thin films were restricted to a narrow range of x: $0.72 \leqslant x \leqslant 0.83$ yet show considerable and nonmonotonic variation of their transport properties with Ta concentration. This behaviour is consistent with a local minimum in the density of electronic states at the Fermi level, as calculated for the rock salt intermetallic Ta$_4$N$_5$, and a rigid band model for describing the transport. The temperature dependence of the resistivity is best fit to the unusual form $\exp(-T/T_0)$. Interestingly enough, the fit parameter T_0 correlates well with the temperature of the maximum of the corresponding thermopower. Both of these characteristics, the fit and the correlation with the thermopower, are consistent with the Jonson–Mahan many-body formalism for charge and thermal transport when one has a nontrivial temperature dependence of the chemical potential. At the lowest temperatures measured, we have also found that the resistivity and thermopower show signatures of electron–electron interactions. We discuss also our results in the light of some theories usually used for describing transport of thin films and to other experimental investigations that have been performed on Ta$_x$N.

1. Introduction

Investigations of the metal–insulator transition (MIT), an as yet unsolved problem in solid state physics, are stimulated by an increase in the availability of various kinds of thin-film samples. Some of these thin films already serve in various applications and newly produced ones have, by properly tailoring their electronic and topological structures, potential to be used in new applications. The vicinity of the MIT is interesting in applications because a small change of the film parameters can considerably change the electronic properties, thereby allowing for externally tuneable devices. Hence, it is important to understand the underlying physics in order to produce desired characteristics of thin films.

In the work presented here, we examine transport properties on a number of different samples of Ta$_x$N, and we find anomalous behaviour which does not fit within the realm of most conventional theoretical descriptions of disordered and strongly correlated materials. Similar effects have been seen before in some amorphous materials where mainly resistivity was measured and discussed. Here, we added the thermopower measurements to give a better insight into underlying physical mechanisms governing the interesting properties we revealed.

Ta$_x$N is already used as a diffusion barrier in copper interconnects on Si chips [1] and as compact thin-film resistors [2]. Also, it has been shown to hold promise as a barrier material in NbN-based Josephson junctions for use in superconducting digital circuits, when it is grown with a resistivity near the MIT [3, 4]. A theoretical understanding of what governs the behaviour of Ta vacancies (which are pentavalent acceptors) and how they affect the physical characteristics of disordered Ta$_x$N was recently

completed [4–6]. It was concluded that the doping and disorder due to the Ta vacancy trigger the MIT transition. These investigations were performed on Ta_xN thin films grown on a crystalline sapphire substrate and on SiO_2-coated Si wafer, which is an amorphous substrate. The transport properties were reported only for the thin films grown on top of sapphire. Here, we present measurements of the transport properties of the thin films grown on the SiO_2-coated Si wafers. A complete comparison between these two sets of experimental data cannot be performed, because the concentration range of Ta on the sapphire substrate was from $x = 1.2$ to $x = 0.43$, which spans the critical concentration, $x = 0.6$, of the MIT, while those on the amorphous substrate vary over a much narrower range of concentrations; from $x = 0.72$ up to $x = 0.83$ which does not include the critical concentration. In addition, the thermopower, which shows interesting temperature dependence, was not measured below room temperatures down to 4 K. Nevertheless, even in such a small range, the concentration variation of the measured physical quantities is considerable and quite interesting. It should be noted that, by varying the growth conditions (the partial pressure of N_2), as it was described in [4–6] and here in short in section 2.1, the concentration range where the monocrystalline Ta_xN rock salt structure was formed in the samples is much narrower if deposition was done on amorphous SiO_2 substrate than if it was done on crystalline sapphire substrate.

In this work, we present measurements of the resistivity and thermopower in the temperature range spanning $\sim$4–320 K. The results are surprising because we find both a strong concentration dependence to the transport and we find a temperature dependence of the resistivity that is fit well by an *exponential in temperature* $\exp(-T/T_0)$. This is an unusual functional form for describing resistivity, but it can be further correlated with the maximum in the temperature variation of the corresponding thermopower. Namely, although the resistivity is a monotonic function of temperature, the thermopower shows a more complicated variation. But, interestingly enough, it assumes a broad maximum near the temperature T_0 used as a parameter in the resistivity fits. Moreover, the derivative of the conductivity ($\sigma = 1/\rho$) with respect to temperature also correlates well with the thermopower: showing a maximum near $T_0 \approx 100$ K and showing a minimum at the lowest temperatures, just as the measured thermopower does. Such a close and simple correlation between resistivity and thermopower in so wide a temperature range (from 4 K to 330 K) is one of our interesting observations, to our knowledge, not seen so far. It should be emphasized that there is not much thermopower data for similar systems (below room temperature), hence this work presents an opportunity to try to explain both the resistivity and thermopower by the same theory. We show that within the general Jonson–Mahan many-body formalism [7, 8] for charge and thermal transport, such an exponential dependence on temperature for the resistivity and the broad maximum for the thermopower are consistent with each other, if one chooses a special temperature dependence to the chemical potential with temperature.

To put our results in the context of conventional approaches, and because we do not have a microscopic model that yields the required temperature dependence of the chemical potential, we also discuss our data within standard theoretical models for thin films, for, so-called, dirty metals and for heavily doped semiconductors near MIT. In particular, we find that at the lowest temperatures measured, below 20 K, the resistivity and thermopower are governed by electron–electron interactions.

We also show that the nonmonotonic concentration dependence of the transport can be understood by examining the density of states of Ta_4N_5 calculated from first principles [5, 6], assuming a rigid band model for concentrations close to $x = 0.8$ and assuming that the density of states of the samples is similar to that of the periodic Ta_4N_5 phase at $x = 0.8$.

2. Experimental methods

2.1. Deposition details

Ta_xN is synthesized in a high-vacuum sputtering system equipped with a dc magnetron sputter gun (model Torus 2C, Kurt Lesker Co.) containing a 99.5%-pure 5.1 cm diameter Ta target. Two types of substrates are used: 1 cm^2 (0 0 0 1) sapphire and 10.2 cm diameter (1 0 0) Si wafers coated with a 140 nm thermal SiO_2 layer. In our experiment, a mixture of N_2 and Ar is used as the sputtering gas. The concentration of Ta in these thin films depends mainly on the partial pressure of N_2 and on the temperature of the substrate during the deposition process. In the case of the Si wafers, the partial pressure was varied from 50 to 100 mTorr while the temperature was kept constant at 450 °C. Thus, we expect that the dynamics of the processes during the cooling to room temperature were the same for each thin-film sample even though the concentration varied. Rutherford backscattering spectroscopy was used to determine the chemical composition and film thickness.

2.2. Room temperature resistivity

For the resistivity measurements, the samples were cut into pieces of size 5 mm × 1 mm. The voltage probe and current sourcing Cu wires ($\Phi = 40\,\mu$m) were affixed to the sample with silver paint. The width of the silver paint was up to 0.5 mm and introduced the greatest error in the determination of the resistivity calculated according to Ohm's law: $\rho = (V/I)(ab/l)$, where ρ is the resistivity of the sample, V is the voltage, I is the current, l is the distance between the voltage contacts, b is the width and a is the thickness of the sample.

The resistivity was also measured by a commercial four point probe instrument with a probe spacing of 0.1 cm (Kulicke and Soffa (Jandel)). The current was linearly increased in 5 mA steps up to 60 mA and the mean value of the sheet resistance, R_{sq}, was calculated for a given concentration. In this interval of current, Ohm's law was also satisfied. The resistivity was then calculated by the following relation: $\rho = R_{sq}a$. The experimental procedure with a comparison between the two described methods was recently used in investigations of Si : B thin films [9]. Independently, the resistivity was also measured on another cut sample but in the van der Pauw geometry. All
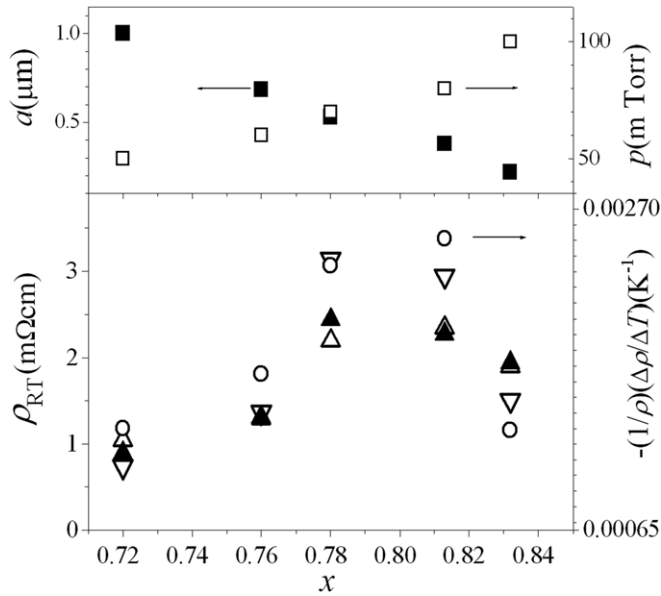
J. Phys. D: Appl. Phys. **43** (2010) 445405

M Očko *et al*

Figure 1. Room temperature resistivity, ρ_{RT}, versus concentration, x, measured by the four contact method (open down triangles), four point probe (closed up triangles) and in the van der Pauw geometry (open up-triangles). Note the agreement between the data for the two commercial methods. The four point method is also in good agreement, although the sizes of the samples were much smaller than those used for the first two methods.
The open points plot the negative temperature coefficient of resistivity (TCR) $(1/\rho)(\Delta\rho/\Delta T)$ at room temperature versus the concentration x. They show almost the same concentration dependence as ρ_{RT}. In the upper inset, we show how the film thickness a depends on the concentration (closed squares—the left-hand scale). The N_2 partial pressures for each concentration obtained (open squares—the right hand scale) are shown with open symbols.

three sets of the room temperature resistivity measurements are displayed in figure 1 (lower part). Good agreement amongst the data is obtained and we can infer, considering all the sets of the data, that the resistivity depends on the chemical composition with a maximum near $x = 0.78$. The differences amongst the data for a given concentration/sample come from the different measurement methods used for the resistivity and they are not due to the inhomogeneity of the electrical properties across the different wafers.

In the upper inset of figure 1, the thickness a versus the chemical concentration is also shown. The N_2 partial pressure used in the sample preparation for each sample chemical composition is also illustrated.

2.3. Microstructural investigations

As reported in earlier publications [5, 6], x-ray diffraction and high-resolution cross-sectional transmission electron microscopy (TEM) were used in the investigation of both kinds of samples: the samples where the deposition of Ta_xN is done on the sapphire (Al_2O_3) substrate and on the SiO_2 one. X-ray diffraction indicates that the synthesized films are composed of Ta_xN in a rock salt structure oriented along the $\langle 1\,1\,1 \rangle$ growth direction. It was observed that the Bragg reflections are broader for concentrations on the N-rich side with respect

to the ones on the Ta-rich side. This fact is consistent with the TEM analysis. Samples on the N-rich side have a ~ 5 nm subgrain mosaic structure with misorientations on the order of $\sim 5°$. The TEM images of the sample for $x = 0.66$ where the deposition is done on sapphire (Al_2O_3) and for $x' = 0.8$, nominally, i.e. $x = 0.81$, as measured, where the deposition is done on the SiO_2 substrate, are shown in figures 2(*a*) and (*b*) respectively. Here we point out that the crystal structure and even the subgrain structure of these two very different samples of the Ta_xN thin films are surprisingly similar [6]. As we had investigated the samples with the concentrations below $x = 1$, these results of the structure and microstructure investigations lead us to conclude that the transport properties measured depend mainly on the concentration x, i.e. on the chemical composition and not on the substrate.

2.4. Measurements of the transport properties

For the thermopower measurements, the films were cut into pieces of size 5 mm long and 1 mm wide with each end in direct thermal contact with a heater. The samples for the resistivity measurements were already described earlier. The thermovoltage Cu wires ($\Phi = 40\,\mu m$) were sealed onto each sample with silver paint. Both samples, usually of the same concentration, were mounted in a calorimeter, which is then put into a liquid He/N cryostat for the low-temperature measurements. The temperature dependence of the resistance from 320 K down to 2 K was measured by the dc technique (Keithley nanovoltmeter K-181, Yokogava current source). The temperature was read from a RhFe thermometer and the measurements were fully automated. More details on the thermopower and resistivity measurement techniques are given in [10].

Measurements of the thermopower on these samples were more difficult, especially at the lowest temperatures, when compared with thermopower measurements of ordinary metallic alloys with much lower resistivities. Therefore, for some concentrations, we do not show any low-temperature data, because the results are not trustworthy. In addition, the magnitude of the thermopower of Ta_xN is quite small below 100 K and, for some concentrations, in the whole temperature interval measured (see, for example, for $x = 0.72$). In these cases, the data are not as reliable as in cases when the thermopower is larger in magnitude. One has to recall that the measured thermovoltage consists of the thermovoltages generated in the sample and in the thermovoltage wires (in our case they were pure, well calibrated Cu wires): $U_{measured} = U_{Cu} - U_{sample}$. The thermovoltages of the Cu wires are small (increasing nonlinearly from $0\,\mu V\,K^{-1}$ at zero temperature to $1.8\,\mu V\,K^{-1}$ at room temperature). The measured thermopower for $x = 0.72$ is even lower in magnitude. Therefore, this sample has a much reduced signal-to-noise ratio than the other samples, which is likely to be the reason why the measured temperature dependence of the thermopower of this sample differs from the results of the other concentrations.
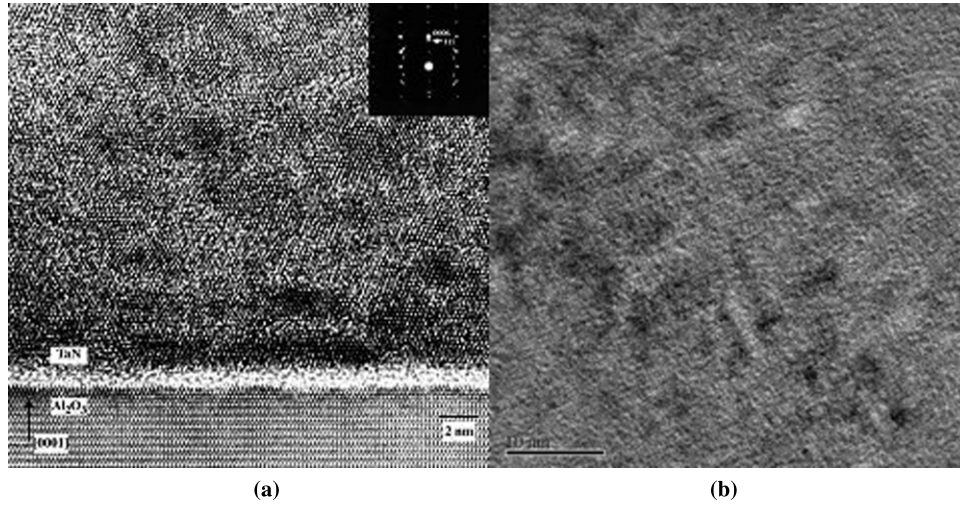
Figure 2. (*a*) Cross-sectional TEM image and selected area diffraction pattern (inset) of a nitrogen-rich $Ta_{0.66}N$ film grown on sapphire. The material has a $\sim$5 nm subgrain mosaic structure with misorientations on the order of $\pm5°$ (as most easily seen in the diffraction pattern). The predominant in-plane epitaxial orientations are $TaN(1\,1\,1)\|Al_2O_3(0\,0\,1)$ and $TaN(1\,\bar{1}\,1\,0)\|Al_2O_3(1\,\bar{1}\,0\,0)$. In the figure, one can see both the substrate and the deposited Ta_xN film. (*b*) Cross-sectional TEM image of a nitrogen-rich $Ta_{0.80}N$ film grown at 450 °C in 4.9 mTorr N_2 partial pressure on an oxidized Si wafer. The material also has a $\sim$5 nm subgrain mosaic structure.

3. Experimental results

In figure 1, we also plot the negative value of the TCR at room temperature, $(1/\rho)(\Delta\rho/\Delta T)|_{RT}$, versus concentration x (open circles). Note that there exists a correlation between the resistivity at room temperature and the TCR at room temperature. This correlation is called the Mooji empirical rule for disordered systems [11]: namely for room temperature resistivities larger than $150\,\mu\Omega$ cm, the TCR is negative and the absolute value increases with resistivity. The accordance of our data with the Mooji rule (in such a small concentration interval with relatively small resistivity change) indicates that the samples are of good quality. The discrepancy at $x = 0.81$ is much smaller if we instead use the results for the resistivity at room temperature that are obtained by the two commercial methods of measurement as discussed in section 2.2.

In figure 3, we plot the ratio of the temperature dependent resistivity to the resistivity at room temperature, $\rho(T)/\rho_{RT}$, for Ta_xN as a function of temperature. For all concentrations, the resistivities show a nonmetallic temperature dependence, i.e. they are, as expected, in an insulating regime of the MIT where the resistivity decreases as the temperature increases (although it does not appear to diverge as the temperature approaches zero as expected for a true insulator). We show that a function of the form

$$\rho(T)/\rho_{RT} = A + B\,\exp(-T/T_0) \qquad (1)$$

describes well the resistivity data of Ta_xN in a wide temperature interval. The extracted parameters are given in the inset of figure 3. Interestingly enough, this expression (1) can also fit the resistivity data of amorphous Zr_xNi_{1-x} alloys from the room temperature down to about 4 K [12]. It was shown that the same function also fits the resistivity of $Fe_xNi_{1-x}P_{14}B_6$ amorphous alloys below the resistivity minimum [13]. The similarity of our system to amorphous Zr_xNi_{1-x} and $Fe_xNi_{1-x}P_{14}B_6$ also holds with respect to the Mooji rule. Mizutani suggested that amorphous materials

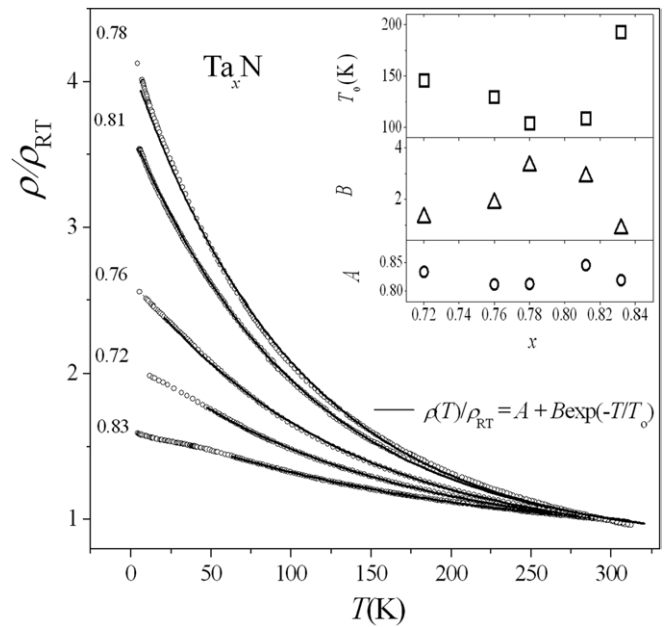**Figure 3.** Temperature dependence of the resistivities represented by the relative resistivities $\rho_r(T) = \rho(T)/\rho_{RT}$ of Ta_xN thin films. Open circles are the experimental data while the solid lines are the best fits to the exponential function: $\rho_r(T) = A + B\,\exp(-T/T_0)$. In the inset, the fitting constants A, B and T_0 are plotted versus concentration.

with high resistivity could be and should be fit by equation (1) [14]; one major pitfall to this procedure is there is no known microscopic mechanism that generically yields such a form. In section 4.7, we show that equation (1) is consistent with an exact Jonson–Mahan formalism for transport, but only when the chemical potential has a rather special dependence on temperature [7, 8].

At the lowest temperatures, the resistivity shows signatures of electron–electron interactions, which are discussed in section 4.5.
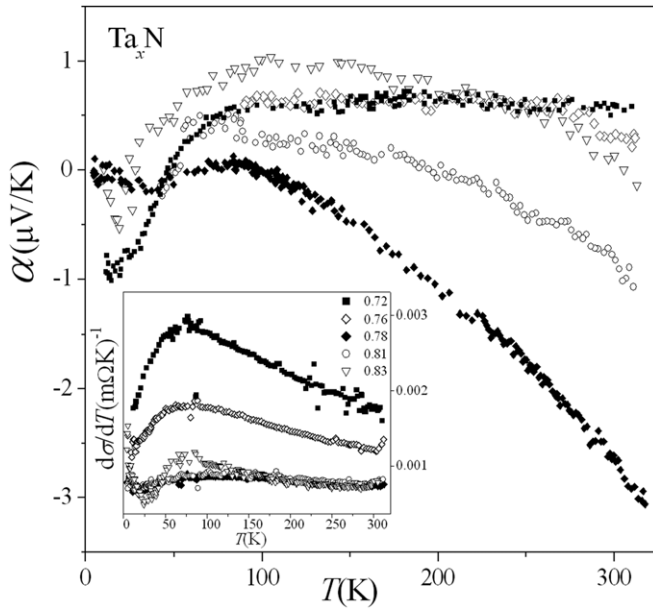
J. Phys. D: Appl. Phys. **43** (2010) 445405

M Očko *et al*

Figure 4. Thermopower of Ta$_x$N thin films. In the inset, the derivatives of the conductivities ($\sigma = 1/\rho$) of Ta$_x$N are presented in order to show the connection between the resistivity and thermopower. The derivative of the conductivity produces all the main features of the thermopower: a wide maximum at higher temperatures and a minimum at low temperatures.

In figure 4, the thermopower of the Ta$_x$N thin films versus temperature is displayed. The temperature dependence of the thermopower appears quite different from the temperature dependence of the corresponding resistivity. A maximum around 100 K appears, while the resistivity increases monotonically with temperature down to the lowest temperatures measured. However, interestingly enough, one can note that the extracted constants T_0 for the exponential fit to the resistivity data correspond well to the thermopower maxima. Furthermore, from the inset of figure 4, where the derivative of the conductivity ($\mathrm{d}\sigma/\mathrm{d}T$) is shown, one can conclude that there exists a correspondence between the conductivity and thermopower data. The maximum of the derivative of the conductivity, $(\mathrm{d}\sigma/\mathrm{d}T)_\mathrm{M}$, is, however, somewhat shifted from the thermopower maximum. The position of the maximum can be obtained from the expression $\mathrm{d}^2[1/(A + B\exp(-T/T_0))]/\mathrm{d}T^2 = 0$. Solving for the temperature of the maximum yields $T \approx T_0 \ln(B/(A + B))$. Using the parameters from the inset of figure 3 in this relation shows that the maximum should be larger for lower concentrations just as shown in figure 4 (and in the inset).

In addition, the derivative $\mathrm{d}\sigma/\mathrm{d}T$ displays minimum at the lowest temperatures, as the thermopower does. This behaviour is attributed to electron–electron interactions as discussed in section 4.5.

Still another correlation between the resistivity and thermopower data can be seen from figure 5. Here, the correspondence is with respect to the chemical concentration. In the inset of figure 5, we show the ratio of the resistivity at 4.2 K, $\rho_{4.2}$ to the resistivity at room temperature, ρ_RT, (circles) together with the negative value of the thermopower at room temperature, α_RT, (squares) versus the concentration x. Both
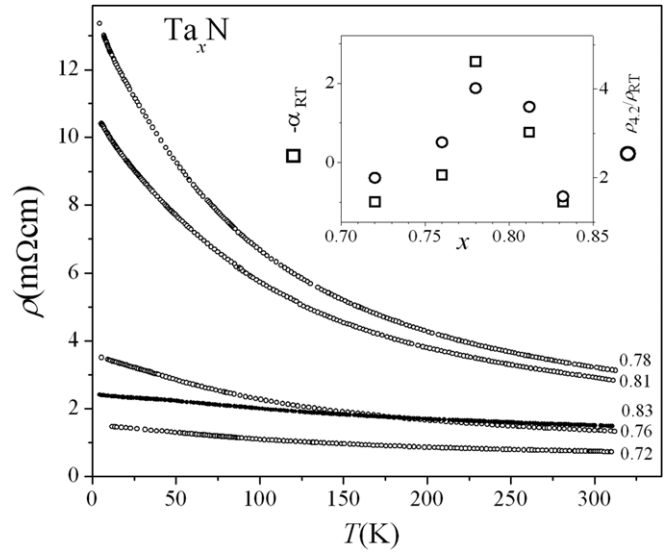

Figure 5. Temperature dependence of the resistivity versus concentration. Note the much stronger temperature dependence of the resistivity for $x = 0.78$ and 0.81 versus other concentrations. In the inset, we plot the ratio of the resistivity at 4.2 K, $\rho_{4.2}$, to the resistivity at room temperature, ρ_RT, (circles) together with the negative value of the thermopower at room temperature, α_RT, (squares) versus concentration.

of these quantities have maxima at $x = 0.78$, just as the room temperature resistivity does. In the main panel of figure 5, we also plot the resistivities in order to point out the difference between the resistivities for $x = 0.78$ and 0.81 and the other concentrations.

4. Theoretical discussion

4.1. Concentration dependence

Besides the temperature dependence of the resistivities and thermopowers of Ta$_x$N ($0.72 \leqslant x \leqslant 0.83$) they show interesting dependence on concentration. Namely, one expects that the resistivity would increase with decreasing x, i.e. with increasing the number of Ta vacancies leading finally to the MIT transition at $x = 0.6$ [5, 6]. In addition, the number of available conducting electrons decreases with x. However, our experiments in the narrow concentration range investigated do not show this generic behaviour. Neither the resistivity (figures 3 and 5) nor the rate of temperature change of the resistivity (figures 1, 3 and 5) is monotonic functions of x. It is interesting, further, that both of these physical quantities have the same concentration dependence and have a maximum at about $x = 0.8$.

To explain such behaviour, we argue that near $x = 0.8$ a 'commensuration effect' exists: if the tantalum vacancies order themselves in a periodic fashion, a sharp dip in the density of states $g(\varepsilon)$ is then formed near the Fermi energy, E_F, as is often seen in the band structure of stoichiometric intermetallics calculated by density functional theory (rigorously speaking, we only need the system to be described by a rigid band model with a dip in the density of states near $x = 0.8$ for this argument to hold; the presence of actual periodic order

is not a requirement). It is known that Ta_4N_5 ($x = 0.8$) is a stoichiometric intermetallic compound which crystallizes in the rock salt structure. The band structure calculations show a sharp dip in $g(\varepsilon)$ at E_F (see figure 2(*e*) in [5]). One may expect that, in the Ta_xN alloy system near $x = 0.8$, the band structure is similar. The effect of reducing the electron number due to the dip in $g(\varepsilon)$ is responsible for a larger resistivity according to the simple Drude picture for conduction:

$$\rho = m_e/Ne^2\tau, \tag{2}$$

where N is the electron concentration, m_e and e are the effective electronic mass and charge, respectively, and τ is the relaxation time. Note that the samples do not need to actually form the periodically ordered phase for this explanation to hold. It will also hold if the system is described well by a rigid band model for doping about the commensuration point, as one fixes the density of states in that case and changes the chemical potential to describe the doping. Such a simple physical picture can explain the experimental results: the resistivity is the largest when the Fermi energy E_F is near the minimum of the density of states $g(\varepsilon)$, i.e. for $x = 0.8$.

It is more difficult to explain the thermopower in such a simple fashion because the thermopower is very small and it changes the sign as the temperature is increased. According to Mott's relation for thermopower one has

$$\alpha \propto \frac{1}{g(\varepsilon)} \frac{\mathrm{d}g(\varepsilon)}{\mathrm{d}\varepsilon},$$

for the low-temperature limit, so one would conclude for this Ta_xN system that the minimum of the density of states is also near $x = 0.80$, but it is difficult to quantify this because the low-temperature thermopower becomes too small at the lowest temperatures to see the concentration range for the sign change. In addition, one might think that the results for $x = 0.72$, which also has a negative thermopower, has the wrong sign to fit the rigid band model. We think this sample is probably doped too far for the rigid band model to hold any more, as we expect the thermopower to once again be negative as we approach the MIT from concentrations above $x = 0.6$. Since the temperature range for the sign change is low, one would need the rigid band model to have a sharp dip in the density of states near the minimum, and indeed the calculated $g(\varepsilon)$ does have a very sharp dip in $g(\varepsilon)$ at E_F (see figure 2(*e*) in [5]).

As we discuss below (equations (18) in section 4.7), a simple analysis provides the following general rule: if the resistivity is large, then the higher temperature thermopower is large. This rule may explain the fact that the maximal thermopowers in our case are for $x = 0.78$ and 0.81. The large thermopower arises from finite-temperature effects where the asymmetry of the density of states plays a significant role (at low temperatures, the thermopower is small near the minimum of the density of states). Hence, under the assumption of a rigid band model near $x = 0.8$, we can explain the gross features of the concentration dependence of the resistivity and thermopower of Ta_xN ($0.72 \leqslant x \leqslant 0.83$) as being primarily due to a dip in the density of states near the Fermi level.
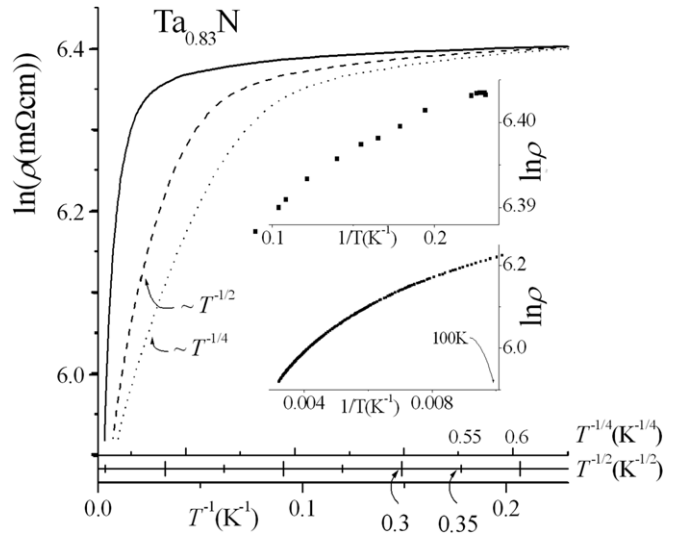

Figure 6. In this plot, we show that the resistivity of Ta_xN thin films cannot be explained by an activation process: $\rho \propto \exp(\Delta/T)$, by a tunnelling process (CELT): $\rho \propto \exp[(W/T)^{1/2}]$ or by the VRH theory: $\rho \propto \exp[(T_{VRH}/T)^{1/4}]$. The resistivity data for the alloy with $x = 0.83$ are shown on a plot with $\ln\rho$ on the vertical axis plotted against $1/T$ (the full line), $1/T^{1/2}$ (the dashed line) or against $1/T^{1/4}$ (the dotted line) on the horizontal axis. The two insets show Arrhenius plots over different temperature ranges to see if activated behaviour ever occurs in the system.

4.2. Negative TCR and the thermopower

For all concentrations of Ta_xN investigated, the resistivities show insulating behaviour with respect to temperature, i.e. the resistivity increases with decreasing temperature or the TCR:

$$\mathrm{TCR} = \frac{1}{\rho} \frac{\Delta\rho}{\Delta T} \tag{3}$$

is negative for all concentrations and temperatures measured. In what follows, we discuss some theories that yield a negative TCR and the application of those theories to our experimental results.

Even though our resistivity data all show a negative TCR, the temperature dependence does not show activated behaviour from an insulating gap:

$$\rho \sim \exp(-\Delta/T). \tag{4}$$

An Arrhenius plot is shown in figure 6 for $x = 0.83$. The plot of $\ln\rho$ versus $1/T$ indicates that the standard activated transport in equation (4) cannot fit the data for a similar range of temperatures as equation (1) can. In the insets we show that activated behaviour is also not seen for higher and lower temperatures. In addition, if equation (4) was valid, the thermopower would behave according to

$$\alpha \sim \Delta/T, \tag{5}$$

which has a strong temperature dependence at low temperatures. Figure 4 shows that the thermopower does not have this form for its temperature dependence.

A negative TCR can also be obtained within Ziman's theory primarily devoted to liquid metals [15]. This theory

is also applicable to amorphous metals, for which the Mooji empirical rule is valid. From this theory, one finds that corresponding thermopower becomes positive and has linear temperature dependence when the TCR becomes negative [16]. Thus, it is obvious that this theory is not applicable to our case even though Ta$_x$N certainly has disorder.

Ta is a transition metal element with an open d shell, but it is unlikely that Ta$_x$N has significant Kondo scattering. While the Kondo effect does yield a negative TCR, it also usually produces sharp peaks in thermopower. In our case, the thermopower is moderate in magnitude, with broad peaks, and hence unlikely to be caused by Kondo physics.

4.3. Inhomogeneity of samples

It is common when working with thin films that experimental results have more sample-to-sample dependence because the properties of the films depend on the process of sample preparation, on the temperature of deposition, on the way the crystal grows, on the sample thickness, the sample profile, its homogeneity, etc. The profile of a sample typically consists of two different zones: the chill zone near the surface and the columnar zone which stretches perpendicularly to the surface inside the sample. In the chill zone, samples are usually homogeneous, but there might be amorphous material between the columns. Therefore, electrons should tunnel from column to column which produces a negative TCR; this may be treated as an inhomogeneity on the mesoscopic scale. The resistivity due to such tunnelling can be described by the charge-energy-limited-tunnelling (CELT) model [17]:

$$\rho \sim \exp[(W/k_{\mathrm{B}}T)^{1/2}], \tag{6}$$

where W is the charging energy. In [18], it is shown that this function describes the resistivity of their Ta$_x$N samples above 20 K. In figure 6, we show that this function does not fit our data. This suggests that, for our samples, columnar zones, if they exist, are not significantly important in the transport. In addition, the upper part of figure 1 shows that the thickness a of our samples increases with decreasing x. If the CELT model was appropriate for our samples, one would expect that resistivity to increase with decreasing x according to the CELT.

In section 2.3, it is shown that our samples are inhomogeneous on a nanoscopic scale. One can expect in such a case that the resistivity can be fit by some variation of Mott's variable range hopping (VRH) model [18, 19]:

$$\rho \sim \exp[(T_{\mathrm{VRH}}/T)^s], \tag{7}$$

where the exponent s satisfies $s = 1/4$ if one is dealing with a three-dimensional material. The exponential behaviour comes from the assumption that there is a difference between the energies of the initial and final state of a scattered electron. Figure 6 shows that equation (7) does not fit our data. This means that the electronic mean free path is smaller than the size of the inhomogeneity. In figure 6, we show that the resistivity cannot be fit by equation (4) (full line), by equation (6) (dashed line) or by equation (7) (dotted line). This is illustrated explicitly for the $x = 0.83$ alloy, but also holds for all the concentrations investigated. Hence the transport must be described by a different microscopic model.

4.4. Weak localization

In cases where disorder dominates the transport, the system is typically described by weak localization theory if the disorder is not too strong. The existence of a negative TCR can be attributed to the interplay of localization and delocalization processes. Anderson showed that, in a sample with disorder where the size of the sample was large enough ($L \to \infty$), electrons would be localized due to quantum coherence. Hence, the net conduction at zero temperature would be zero even in the case when the density of states at the Fermi level is not zero [20]. But in real systems, the size of the samples is limited and electrons can reach the second electrode after a finite number of scattering events. The scaling theory for weak localization deals with the relation between the sample size (L) and the dimensionality (d) of a sample and how they determine the conductivity of the sample when quantum coherence is taken into account [21, 22]. The conductivity in the 3D case can be expressed for $L > \ell$ in the form [23]

$$\sigma_{\mathrm{3D}}(L) = \sigma_0 - \frac{e^2}{\hbar\pi^3}\left[\frac{1}{\ell} - \frac{1}{L}\right], \tag{8}$$

Where ℓ is the elastic mean free path and σ_0 is the contribution to the conductivity calculated in a classical way (equation (2)). According to relation (8) and a simple mathematical calculation, with increasing L, σ would be decreased. The second term (the first one in the bracket) arises from quantum interference effects; it decreases the conductivity. Equation (8) is valid at $T = 0$. With increasing temperature, inelastic scatterings appear which destroy the quantum coherence. If $\tau_{\mathrm{in}} \gg \tau_{\mathrm{e}}$ (9), an electron diffuses the distance

$$L_{\mathrm{Th}} = (D\tau_{\mathrm{in}})^{1/2}, \tag{9}$$

where L_{Th} is Thouless distance. Within L_{Th}, coherence is maintained. D is the diffusion constant, τ_{in} is the inelastic relaxation and τ_{e} the elastic relaxation time. We note here that the effective dimensionality of a system is the number of dimensions for which the sample size is larger than the Thouless distance:

$$L > L_{\mathrm{Th}}. \tag{10}$$

Assuming

$$\tau_{\mathrm{in}} \propto T^{-p}, \tag{11}$$

where p depends on scattering mechanism, taking $L \propto L_{\mathrm{Th}} \propto \tau_{\mathrm{in}}^{1/2} \propto T^{-p/2}$ one then finds

$$\sigma_{\mathrm{3D}}(T) = \sigma(0) + \frac{e^2}{\hbar\pi^3}\frac{1}{c}T^{p/2}, \tag{12}$$

where c is a constant and $\sigma(0)$ is the conductivity at zero temperature comprising the first and second terms of the equation. According to equation (12), assuming that weak localization is the underlying physics which governs the observed temperature dependence of the resistivity/conductivity, it is customary to fit the experimental data to the form

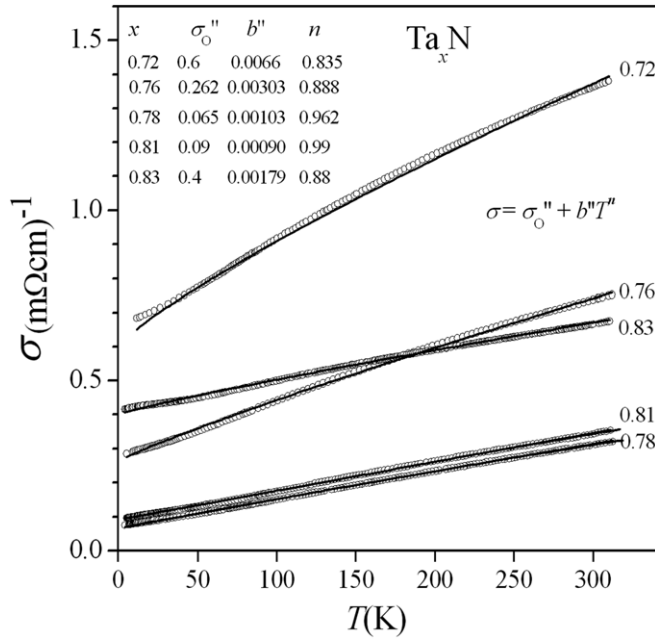$$\sigma = \sigma(0) + bT^n. \tag{13}$$

Figure 7. Conductivity of the Ta_xN thin films versus temperature. The lines represent the fit of the experimental results to the functional form $\sigma = \sigma_o'' + b''T^n$. In the inset table, the fitting constants σ_o'', b'' and n are shown.

The value of the exponent n determines the dephasing mechanism, which primarily destroys the coherence of the elastic scattering, thereby destroying weak localization. There are many theories predicting various dephasing processes under various conditions but here we mention only some which could be candidates to explain the Ta_xN resistivity data. When the dominant dephasing mechanism is electron–phonon scattering, the expected value of p is 3 ($n = 3/2$) [24], while in the case of inelastic electron–electron collisions, p is 2 and 3/2 for the clean and dirty limits [24], respectively. Furthermore, values of n equal to 0.5, 1 and 1.5 have been predicted by Kaveh and Mott for transport dominated by electron phonon scattering for $T \gg T_{Deby}$, electron–electron scattering and electron phonon scattering for $T < T_{Deby}$, respectively [25], However, Dodson *et al* associate $p = 2$ with electron–phonon scattering [26]. Clearly, a consensus has not been reached as to the value of n expected for each dephasing mechanism.

Fitting the Ta_xN data to equation (13), [5, 6] found that n lies between 1 and 1.2 for most films deposited on sapphire. These values fall within a range found for a number of films reported in the literature, including 0.84 for AuGe alloys [26], 1.2–1.65 for composite Al–Ge films [27], 0.3–0.7 for Si doped with P [28, 29] and 0.5 for Y–Al metallic glasses [30].

In figure 7, we present our data together with the values of the best fits obtained from the relation in equation (6). The exponent n is slightly smaller than 1 implying that the dephasing for the inelastic scattering mechanism might be electron–phonon scattering according to Dodson *et al* [26]. Like the other parameters extracted from our data, n does not show a monotonic change with the concentration, but an extremum near the middle of the concentration interval investigated. The values in this case are very close to 1, within 5%, being 0.95 and 0.99 for $x = 0.81$ and 0.78, respectively.

Typically, an integer value for p is rarely found in experiments. The theoretical relations are certainly oversimplified for application in a wide temperature range. For example, the relation in equation (9), $\tau_{in} \gg \tau_e$ or $\ell_{in} \gg \ell$ might not be completely fulfilled at higher temperatures. This does not imply that there is no quantum coherence and thereby no localization at higher temperatures. This means just that the theoretical description is more complicated. A negative TCR generally indicates that localization still persists, but such a simple relation (as shown in equation (11)) between τ_{in} and T does not. One may argue that just this fact and localization lead to the exponential relation in equation (1), which can fit our resistivities. Namely, figure 7 shows that equation (13) can describe our data relatively well, and with some corrections to equation (13) by changing equation (11) one could eventually lead to equation (1).

We saw in section 4.2 that the thermopower served to further discriminate the applicability of models which could describe the resistivity data. It is not clear how to determine the temperature dependence of the thermopower corresponding to the resistivity in equation (13) as we are unaware of any theory for the thermopower in weak localization. Hence, we now use some different physical models to obtain equation (1), but with the additional requirement that the thermopower must also be explained by the same model (see sections 4.6 and 4.7).

4.5. Electron–electron scattering

Equation (12) was derived under the assumptions of noninteracting particles. Altshuler *et al* [31] took into account the influence of the electron–electron interaction (e–e) in a disordered system. Besides the influence on coherency of elastic processes, there exists an additional contribution of the e–e interaction (like the T^2 term in crystalline systems):

$$\sigma = \sigma(0) + mT^{1/2} + bT^n, \qquad (14)$$

where m can be negative as it is in some highly doped semiconductors [9, 31], but in disordered metallic systems it is usually positive like the third term in equation (14). Plotting the transport data versus $T^{1/2}$ (figure 8) shows the presence of the $T^{1/2}$ term at the lowest temperatures. For $x = 0.83$, the interval of this term stretches to about 20 K (see also figure 9), but for $x = 0.81$ and 0.78 the interval is only up to 11 K. For the data with $x = 0.72$ and 0.76, the lowest measured temperature is too high to see the electron–electron interaction term. The extracted values of m are plotted in the inset to figure 8.

Our data (closed circles) are compared with the results from [18]. Both sets of the data show that the data are mutually comparable and that m decreases with decreasing x. Moreover, both sets of data can be scaled to a theoretical curve for m. In [31], an expression for m is given which was compared with the experimental results in [29]:

$$m \propto 1 - (3/2X)\ln(1 + X), \qquad (15)$$

$$X = (2k_F/\kappa)^2, \qquad (16)$$

where k_F is the Fermi wave number and κ^{-1} the Thomas–Fermi screening length.
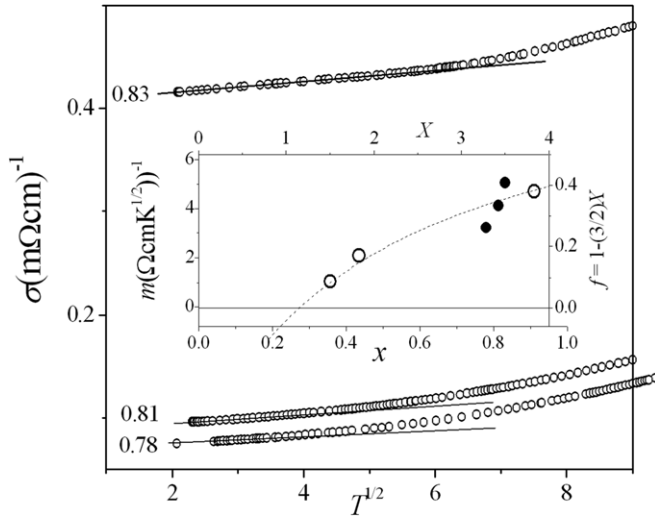
Figure 8. Conductivity at the lowest temperature measured for the $x = 0.78$, 0.81 and 0.83 alloys plotted against $1/T^{1/2}$ in order to reveal the existence of electron–electron scattering. The extracted parameters m are displayed in the inset together with the ms from [18]. The dashed line represents the function f coming from theory which accounts for the contributions of electron–electron scattering to the conductivity ([31]).
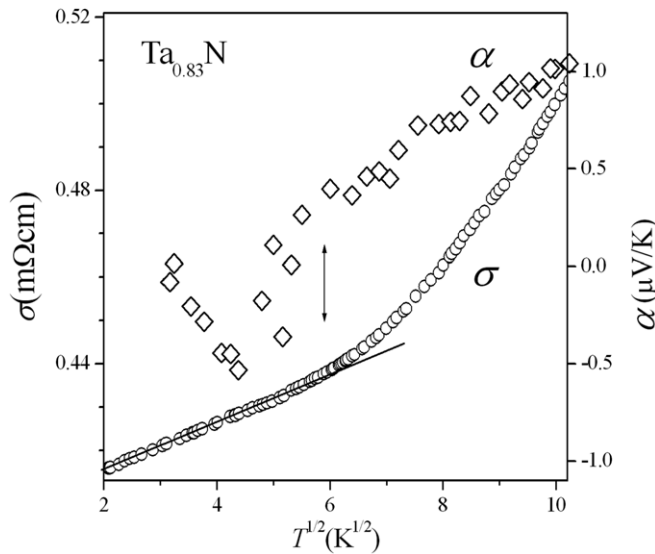

Figure 9. Thermopower and conductivity of the $x = 0.83$ sample plotted against $1/T^{1/2}$ in order to show the temperature range where the electron–electron interaction dominates the transport properties.

The main puzzle that might remain with this conventional analysis is that if localization is the driving physics of these samples, governing the high-temperature behaviour, then why does not the resistivity diverge as the temperature goes to zero? A standard answer within weak localization theory is that the coherence length, ξ, is larger than the dimension of a sample, L. The almost abrupt evolution to the $T^{1/2}$ dependence in the resistivity and the abrupt evolution to the thermopower minimum (figure 9) suggest that the inelastic electron–electron interaction is the mechanism which hinders Anderson localization in the samples we have investigated.

In figure 9, we also plot the thermopower. One can clearly see that the low-temperature peak is occurring in precisely the

temperature range where the system is dominated by electron–electron scattering.

Here we note that [18] also found that the resistivity of the Ta_xN thin films was determined by electron–electron interactions at low temperature (described by the form $\rho = \rho(0) + m'T^{1/2}$). At higher temperatures, the resistivity was described by the CELT model by equation (6). It is not clear to us how the divergence in the resistivity as the temperature goes to zero is avoided or removed by the electron–electron interactions in their samples.

We have one cautionary note to make about how to apply weak localization theory. In many papers, equations (13) and (14) are written in terms of the resistivity instead of the conductivity. The relations have the same form when one assumes $\rho(0) \gg m'T^{1/2}$, $b'T^n$. However, such an approach is flawed because the theoretical equations of weak localization and of electron–electron scattering are inferred in terms of σ and the theoretical interpretations of the exponent m is given in terms of σ; if one instead performs the analysis in terms of resistivity, one can reach incorrect conclusions. For example, in [18], the low-temperature data were fit by $\rho = \rho(0) + m'T^{1/2}$ and the extracted ms were not found to be a monotonic function of x. However, if one calculates m from their data using the power law behaviour for the conductivity (it is easy to show that $m = -m'/\rho(0)^2$), then the inset to figure 8 shows that m is a monotonic function of x. Moreover, these values are in accordance with ours and both data are in accordance with the theory of electron–electron interactions in disordered systems [31].

4.6. Falicov–Kimball model

An alternative picture for describing the scattering due to the Tantalum vacancies is to use the Falicov–Kimball model [32], where the heavy particles are Ta ions and the light particles are the conduction electrons. Since the electrons have a different local site energy when they are on a site with a Ta vacancy versus on a site where a Ta ion lies, the local Coulomb interaction is just between the conduction electrons at site i and the ion at site i; it represents the difference in the site energies between an electron and a Ta ion versus an electron and a Ta vacancy. The local electrons also hop between neighbouring sites in the Falicov–Kimball model, whose Hamiltonian is then

$$H_{FK} = -\sum_{\langle ij \rangle} t_{ij} c_i^+ c_j + U \sum_i c_i^+ c_i w_i, \qquad (17)$$

where we assume for simplicity, just spinless electrons (spin is trivial if the conduction electrons have negligible electron–electron interactions between themselves). The hopping matrix element $-t$ is between nearest neighbours and the symbol w_i denotes the Ta ion concentration at site i. Because the presence of a vacancy reduces the number of electrons in the system, we relate the ion fillings to one minus the concentration of vacancies as $w_i = x$ and the electron concentration as $\rho_e = 0.5 - w_i/6 = 0.5 - x/6$, so the system, with repulsive U, will have a Mott-like MIT at $x = 0.6$ when the interaction is large enough and will be a good metal at $x = 1$; note that there are many different ways one can choose to vary the

fillings with the Ta concentration (especially for the mapping onto an effective spinless single-band model), one just needs to have the electron concentration equal to 0.4 when the Ta concentration is 0.6 to obtain a MIT when the interaction is large enough. This model, including all of its transport properties, can be solved exactly in the infinite-dimensional limit using dynamical mean-field theory and it corresponds to examining annealed averages over the disorder rather than quenched averages of weak localization theory. Details for how this is done appear elsewhere [33]. Unfortunately, it is difficult to get this model to describe the shape of the resistivity versus temperature that is seen in experiment. The insulating behaviour exists only exactly at the critical Ta concentration ($x = 0.6$), and the resistivity will be orders of magnitude higher there than at other concentrations in the numerical calculations (if U is large enough to be beyond the Mott transition). The model does not typically have an exponential dependence of the resistivity on temperature; such a shape is possible to find with finely tuned parameters near the critical interaction for the MIT, but does not remain when doped far enough away from the critical doping (as in the current experimental data). It is possible that the failure of the Falicov–Kimball model to describe this system arises from the lack of localization physics in the model (the Falicov–Kimball model involves an annealed average over the Ta vacancy sites). An insulator is formed only when there is a gap in the density of states, and that always gives rise to thermally activated resistivities, which are huge compared with the nearby metallic cases. The model can produce an insulator-like temperature dependence to the resistivities (negative TCR), where the resistivity decreases as the temperature increases, but not with the correct functional form seen in experiment unless the parameters are fine-tuned. The experimental systems appear to be more like anomalous (non-Fermi liquid) metals—the resistivity rises as T falls, but it does not diverge at $T = 0$, and hence remains conducting (albeit with a large resistivity). This strange temperature dependence along with the fact that the resistivity can be above the minimum metallic resistivity implies the system, if it remains conducting, is an anomalous metal.

4.7. Jonson–Mahan formalism

Our next step in trying to formulate a general theory for the transport proceeds along more basic grounds using the many-body formulation of transport theory via the current–current correlation function and the Kubo formula. Our philosophy is to determine the exact functional form for the transport in terms of the many-body relaxation time. We then use a phenomenological expansion for the relaxation time, based on a simple Taylor-series expansion, to analyse the data. This does not provide a microscopic description of the transport but does show how the charge and heat transport must be interrelated.

When one calculates the charge and heat transport, one can relate the thermopower to the resistivity via the transport integrals and the Jonson–Mahan theorem [7, 8]. Here we find that the resistivity satisfies

$$\rho = \frac{h}{e^2 L_{11}}; \qquad L_{11} = \int \mathrm{d}\omega \left[-\frac{\mathrm{d}f(\omega - \mu)}{\mathrm{d}\omega} \right] \tau(\omega), \quad (18)$$

with $f(\omega - \mu) = 1/[1 + \exp\{(\omega - \mu)/T\}]$ the Fermi–Dirac distribution function and $\tau(\omega)$ the number current–number current correlation function (effective many-body transport relaxation time) including all vertex corrections and summed over momentum. Similarly, the exact expression for the thermopower is

$$\alpha = -\frac{k_B}{|e|T} \frac{L_{12}}{L_{11}};$$
$$L_{12} = \int \mathrm{d}\omega \left[-\frac{\mathrm{d}f(\omega - \mu)}{\mathrm{d}\omega} \right] (\omega - \mu) \tau(\omega) \quad (19)$$

with the same transport relaxation time $\tau(\omega)$ as is used in the L_{11} integral. Instead of developing a microscopic model for the transport relaxation time, we assume that it takes a relatively simple functional form, and then determine what constraints are placed on the equations to yield the observed transport behaviour. This is a phenomenological approach within the confines of the exact many-body theory.

The basic idea underlying our approach is that the Ta vacancies are static defects, and hence we do not expect the transport relaxation time to vary much with temperature in the low-temperature region (after all there is no low-energy scale entering the problem). Using the density of states as a guide, we would find that the transport relaxation time behaves as a constant plus a quadratic in ω, if the imaginary part of the self-energy was taken as a constant. A similar functional form occurs for solutions of the Falicov–Kimball model, where the Ta vacancy positions are annealed over, and the transport relaxation time shape is independent of temperature. Hence, we take as a working ansatz that $\tau(\omega)$ is independent of temperature and behaves like a constant plus a quadratic piece. Then the integrals for the transport can be performed immediately, and they yield the following results:

$$L_{11} = \tau_o + \frac{\mu^2}{2} \tau_o'' + \frac{\pi^2}{6} T^2 \tau_o'', \qquad L_{12} = \frac{\pi^2}{3} T^2 \mu \tau_o'', \quad (20)$$

which hold as long as the Fermi temperature window is much smaller than the frequencies where the quadratic approximation $\tau(\omega) = \tau_o + \tau_o'' \omega^2/2$ holds for the transport relaxation time. The chemical potential μ will be equal to zero at the minimum of the relaxation time, which occurs near $x = 0.78$. Since the chemical potential in a metal approaches its zero temperature limit quadratically, we immediately learn that at low enough temperature, if the system is metallic, then we must have the resistivity approach a constant value quadratically in temperature, and the thermopower approaches zero linearly in temperature (note that this does not require the metal to be a Fermi liquid or to have a positive TCR). We expect there to be a sign change in the low-temperature thermopower at the critical concentration ($x = 0.78$) where the transport relaxation time has a minimum. The data are not inconsistent with this observation, although the thermopower is so small, it is difficult to achieve trustworthy experimental results in this regime. We should also note that the simplified form of the transport relaxation time does not describe the low-temperature electron–electron interaction regimes described

in section 4.5. One might ask why the thermopower at low temperature is negative for both the $x = 0.83$ and $x = 0.72$ cases because we would expect one to be electron-like and one to be holelike since they are on opposite sides of the point where we expect to see a minimum in the effective density of states. One possible explanation within this framework is that the case with $x = 0.72$ is already close enough to the MIT at $x = 0.6$ that it is beginning to show the electron-like behaviour at low temperature. The other explanation is, of course, that the many-body relaxation time has a much stronger dependence on concentration than we assumed above (and it could also have a temperature dependence due to the electron–electron interaction).

If we now take a phenomenological point of view to analyse the transport properties at intermediate temperatures, then we must have the chemical potential behave like

$$\mu(T) = \pm\sqrt{\frac{2}{\tau_o''}\left[\frac{h}{e^2}\frac{1}{A + B\,\exp(-T/T_0)} - \tau_o - \frac{\pi^2}{6}T^2\tau_o''\right]}$$
(21)

in order to have a resistivity that is exponential in temperature $\rho = A + B\exp(T/T_0)$. The behaviour of the chemical potential versus temperature is determined by the density of states—the above form is approximately linear in temperature for a wide range of temperature, which is how the chemical potential behaves at high temperature, so such a form is possible in a realistic system; it is the deviations from linearity that determine the specific functional behaviour at these intermediate temperatures and it is difficult to establish under what conditions such a shape would occur for a given density of states. Furthermore, since the linear behaviour is a high-temperature limit and the exponential behaviour persists down to liquid helium temperatures in the experiments, we find these observations difficult to reconcile with the intermediate temperature limit of the transport theory, especially because the data show limited evidence of a crossover to the expected quadratic temperature dependence for the resistivity at low temperature.

The thermopower becomes

$$\alpha(T) = -\frac{k_B}{|e|}\frac{\pi^2}{3}\frac{T\mu\tau_o''}{\tau_o + (\mu^2/2)\tau_o'' + (\pi^2/6)T^2\tau_o''}$$
$$= -\frac{k_B}{|e|}\frac{\pi^2}{3}[A + B\exp(-T/T_0)]T\mu.$$
(22)

One immediately sees from this form for the thermopower, that the sign of the thermopower is tied to the sign of the chemical potential, since the other temperature-dependent terms are all positive. Hence, if we see a high-temperature zero crossing, then we should see the maximum in the thermopower occur at a lower temperature from the arguments given below (indeed this is seen in the data). With this form for the thermopower, we can now estimate where the extremum of the thermopower lies. Since the chemical potential is approximately linear in this region of temperature, the thermopower has an extremum near the point where the chemical potential vanishes as a function of T if the high-temperature chemical potential has a different sign than the chemical potential in the limit as T goes to zero.

The condition for the extremum is

$$\frac{A}{B}[1 + \exp(-z)]\left[2 - \frac{\mu(z = 0)}{\mu(z)}\right] = z\,\exp(-z),$$
(23)

with $z = T/T_0$. The right-hand side is never larger than 0.368, while the left-hand side is close to $2A/B$ if the chemical potential does not change sign, which is larger than the maximum for the experimental data measured on these samples. The chemical potential obviously changes sign when the argument of the square root vanishes, which typically has two roots or zero roots depending on the size of the different parameters. Since we expect the exponential form of the resistivity to change to a quadratic dependence at low enough temperature, we should find the true resistivity at $T = 0$ to be somewhat smaller than the limiting form of the exponential dependence because it must turn over to have vanishing slope (the true resistivity is inversely related to τ_o). Then the low-temperature extremum of the thermopower will be a constant of order unity multiplied by AT_0/B. The other root is at much higher temperature and is independent of T_0 for the given small value of the curvature of the transport relaxation time. Hence, it is likely that the maximum of the thermopower is correlated with the exponential fit parameter T_0 when the resistivity takes this exponential dependence. The larger temperature dependence, where the thermopower starts to behave linearly, is probably a crossover to the Heikes limit where the thermopower is proportional to the chemical potential which is linear at high temperature.

To conclude, the analysis within the Jonson–Mahan formulism shows (*i*) the maximum in the thermopower can be related to the resistivity and to the fitting constant T_0, if the resistivity obeys equation (1) and (ii) that the α is proportional to ρ when the L_{12} coefficient has small temperature dependence; this can explain the maximal values of the thermopower and resistivity for $x = 0.78$ and $x = 0.81$ (see the inset to figures 1 and 5).

5. Summary

We investigated the low-temperature transport properties of Ta$_x$N ($0.72 \leqslant x \leqslant 0.83$) thin films deposited on the SiO$_2$ amorphous substrate. The transport properties show considerable and nonmonotonic variation with x (figures 1, 5), which we attribute to the appearance of a local minimum in the density of the electronic states at the Fermi level near $x = 0.8$.

The *temperature* dependence of the resistivity is discussed within the context of a number of different models (figure 6). We find that the resistivity data can be fit by the weak localization theory in equation (13) [21–23] (see figure 7). The fitting parameters suggest that the dephasing scattering above 20 K is electron–phonon scattering. However, the parameter p in equation (13) extracted from the data is not an integer as the theory predicts (although it is close to 2). In addition, we could not verify within the weak localization theory, or within any other one we have also discussed, the following experimental findings: (i) we find a much better fit of the resistivity data with an exponential function, equation (1): $\exp(-T/T_0)$

(figure 3); (ii) although equation (1) is a monotonic function, the parameter T_0 is closely related to the nonmonotonic temperature dependence of the thermopower (at about T_0, there is a wide maximum of the thermopower) and (iii) the derivative of $1/\rho$, the conductivity, correlates well with the thermopower showing both a maximum at about $T_0 \approx 100\,K$ and a low-temperature minimum just as the thermopower does (figure 4 and the inset to figure 4). Such a close and simple connection between the resistivity and thermopower in so wide a temperature range (from 4 K to 330 K) is one of the most interesting results of our study; not seen elsewhere.

We show that a phenomenological approach based on the Jonson–Mahan formalism (section 4.7) can describe the resistivity by a complicated temperature dependence of the chemical potential $\mu(T)$ and can also describe the correlation of the resistivity data with the maximum in the thermopower.

At the lowest temperatures measured (up to 20 K for $x = 0.83$), the conductivity data can be explained by Altshuler's theory of electron–electron interaction in disordered system [31] (figure 8). The analysis of the data shows that the low-temperature minimum in the thermopower also arises from electron–electron scattering (figure 9).

Finally, we conclude that the observed transport properties are not due to deposition on the SiO_2-coated Si wafers, but are an intrinsic property of Ta_xN. Nevertheless, it should be noted that, by varying the growth conditions (the partial pressure of N_2), as described in section 2.1, the concentration range where the monocrystalline Ta_xN rock salt structure was formed is much narrower when the deposition was done on an amorphous SiO_2 substrate than if it was done on a crystalline sapphire substrate. The reason seems obvious. The monocrystalline structure is formed on the amorphous substrate only if the concentration is around the stable intermetallic Ta_4N_5. The periodicity of this structure giving the gap in the density of states is responsible for the main features observed in the transport properties of the Ta_xN thin films deposited on the amorphous SiO_2 substrate.

Acknowledgments

References

[1] Kaloyeros A E and Eisenbraun E 2000 *Annu. Rev. Mater. Sci.* **30** 363
[2] Pham A V H *et al* 2002 *IEEE Trans. Adv. Packing* **25** 98
[3] Tsai M H, Sun S C, Lee C P, Chiu H T, Tsai C E, Chuang S H and Wu S C 1995 *Thin Solid Films* **270** 531
[4] Yu L, Gandikota R, Singh R K, Gu L, Smith D J, Meng X, Zeng X T, Van Duzer T, Rowell J M and Newman N 2006 *Supercond. Sci. Technol.* **19** 719
[5] Yu L, Stampfl C, Marshall D, Eshrich T, Narayanan V, Rowell J M, Newman N and Freeman A J 2002 *Phys. Rev.* B **65** 245110-1
[6] Yu L 2006 *Thesis* Arizona State University
[7] Jonson M and Mahan G D 1980 *Phys. Rev.* B **21** 4223
[8] Jonson M and Mahan G D 1990 *Phys. Rev.* B **42** 9350
[9] Žonja S, Očko M, Ivanda M and Biljanović P 2008 *J. Phys. D: Appl. Phys.* **41** 162002
[10] Očko M, Miljak M, Kos I, Park J-G and Roy S B 1995 *J. Phys.: Condens. Matter* **7** 2979–86
[11] Mooji J H 1973 *Phys. Status Solidi* a **17** 521
[12] Očko M *et al* submitted
[13] Babić E, Očko M, Marohnić Z, Schaafsma A S and Vince I 1980 *J. Phys. France* **41** C-473
[14] Mizutani U 1988 *Mater. Sci. Eng.* **99** 165
[15] Ziman J M 1972 *Principles of the Theory of Solids* (Cambridge: Cambridge University Press)
[16] Očko M and Babić E 1989 *J. Phys. France* **50** 3233
[17] Sheng P, Abeles B and Arie Y 1973 *Phys. Rev. Lett.* **31** 44
[18] Lal K, Ghosh P, Biswas D, Meikap A K, Chattopadhyayy S K, Chatterjee S K, Ghosh M, Baba K and Hatada R 2004 *Solid State Commun.* **131** 479
[19] Mott F 1974 *Metal–Insulator Transitions* (London: Taylor and Francis)
[20] Anderson P W 1958 *Phys. Rev.* **109** 1492
[21] Abrahams E, Licciardello D C and Ramakrishnan T V 1979 *Phys. Rev. Lett.* **42** 673
[22] Abrahams E, Lee P A and Ramakrishnan T V 1982 *Phys. Rev.* B **24** 6783
[23] Lee P A and Ramakrishnan T V 1985 *Rev. Mod. Phys.* **57** 287
[24] Schmid A 1974 *Z. Phys.* **271** 251
[25] Kaveh M and Mott N F 1982 *J. Phys. C: Solid State Phys.* **15** L707
[26] Dodson B W, McMillan W L, Moch J M and Dynes R C 1981 *Phys. Rev. Lett.* **46** 46–9
[27] Shoshany J, Goldner V, Rosenbaum R, Witcomb M, McLachlan D S, Palevski A, Karpovski M, Gladkikh A and Lereah Y 1996 *J. Phys.: Condens. Matter* **8** 1729–42
[28] Rosenbaum T F, Andres K, Thomas G A and Bhatt R N 1980 *Phys. Rev. Lett.* **45** 1723–6
[29] Rosenbaum T F, Andres K, Thomas G A and Lee P A 1981 *Phys. Rev. Lett.* **46** 568–71
[30] Cochrane R W and Strom-Olsen J O 1984 *Phys. Rev.* B **29** 1088–90
[31] Altshuler B L, Aronov A G, Khmelnitskii D E and Larkin A L 1982 *Quantum Theory of Solids* (Moscow: Mir) pp 130–237
[32] Falicov L M and Kimball J C 1969 *Phys. Rev. Lett.* **22** 997
[33] Freericks J K and Zlatić V 2003 *Rev. Mod. Phys.* **75** 1333